Springer

Journal of Mechanical Science and Technology 23 (2009) 3323~3331

Journal of Mechanical Science and Technology

www.springerlink.com/content/1738-494x
DOI 10.1007/s12206-009-1019-7

Development of high speed computation algorithm for transient analysis of rectangular plates †

M. S. Choi[1,*], D. J. Jang[1], Y. B. Kim[2], J. S. Jang[2] and D. H. Moon[2]

[1]*Department of Maritime Police Science, Chonnam National University, Yeosu, 550-749, Korea*
[2]*School of Mechanical Engineering, Pukyong National University, Busan, 608-749, Korea*

(Manuscript Received May 3, 2009; Revised September 4, 2009; Accepted September 16, 2009)

Abstract

A new transient analysis method for a rectangular plate structure comprised of a large number of plate elements was developed in order to significantly reduce computational time and memory. This algorithm was derived from the combination of the transfer technique of the transfer mass coefficient method, the modeling technique of the finite element method, and the numerical integration technique of Newmark's method. In this paper, the algorithm for the transient analysis of a rectangular plate structure is formulated by the proposed method. In order to verify the computational accuracy and efficiency of the proposed method, the results obtained by the proposed method were compared with those obtained by the finite element method and the finite element-transfer matrix method. The proposed method, the finite element-transfer mass coefficient method, could considerably reduce the computation time without the loss of accuracy, in spite of using small computation memory, by using the transfer rules successively.

Keywords: Computation time; Finite element method; Newmark's method; Rectangular plate; Transfer mass coefficient method; Transfer matrix method; Transient response

1. Introduction

The finite element method (FEM) is the most powerful and widely used method in the field of computer-aided engineering. However, it requires long computation time and large computation memory for accurately solving dynamic problems of structures that have a number of degrees-of-freedom [1-11]. To overcome the above limitations of the FEM, some numerical methods have been developed and used for computing the transient responses of rectangular plate structures [3, 6, 8].

The combined use of the finite element-transfer matrix method (FE-TMM) was proposed by Dokainish [1] for the free vibration analysis of plates, and the FE-TMM was introduced for analyzing the transient response of frame structures and rectangular plate structures [3, 5]. The advantages of the FE-TMM are a short computation time and an economical computation memory. However, it was pointed out that the recursive multiplications of transfer matrices in the FE-TMM produce the propagation of round-off errors. To minimize these errors in the FE-TMM, we need to use some techniques such as exchanging of the state vectors [3]. However, these techniques counteract the simplicity, which is the merit of the transfer matrix method [12]. Therefore, it is not easy to apply the FE-TMM to the transient analysis of the rectangular plate structures modeled as a number of plate elements.

A new transient analysis algorithm for a rectangular plate structure comprised of a number of plate elements was developed in order to significantly reduce computational time and memory. This algorithm was derived from a combination of the transfer technique of the transfer mass coefficient method [11], the

† This paper was recommended for publication in revised form by Associate Editor Yeon June Kang

*Corresponding author. Tel.: +82 61 659 3183, Fax.: +82 61 659 3189
E-mail address: engine@chonnam.ac.kr

modeling technique of the FEM, and the numerical integration technique of Newmark's method [13]. It is termed the finite element-transfer mass coefficient method (FE-TMCM).

In this paper, the transient analysis algorithm for a rectangular plate structure is formulated by the FE-TMCM. The computational trust and speed of the FE-TMCM are demonstrated by comparing results obtained by the FE-TMCM with those obtained by the FEM and the FE-TMM for several rectangular plate structures.

2. Formulation

2.1 Modeling

As shown in Fig. 1, a rectangular plate structure is considered to be an analytical model used to formulate the transient response analysis algorithm of plate structures.

The plate structure consists of a rectangular plate, elastic springs and viscous dampers that support the plate from the base, as well as added masses. The rectangular plate is divided into *m* strips, and each strip is subdivided into *n*-1 rectangular plate elements, as shown in Fig. 2. The sections dividing or bordering the strips are called nodal lines, which are designated as nodal line 1, nodal line 2, ⋯, and nodal line *m*+1 successively from the left-hand edge to the right-hand edge of the plate.

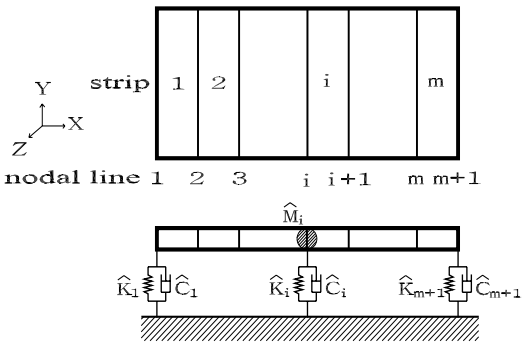

Fig. 1. Analytical model.

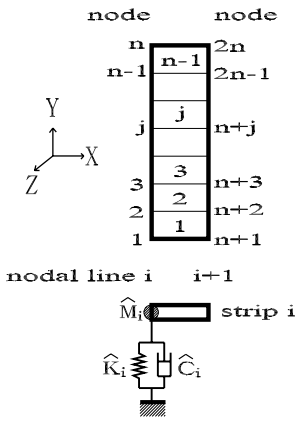

Fig. 2. Strip divided into rectangular plate elements.

Each nodal line has *n* nodes, and a node has 3 degrees-of-freedom for analyzing the bending vibration of a plate. Therefore, each nodal line has 3*n* degrees-of-freedom. The displacement vector of the node *j* ($\mathbf{u}_j = \{u_z, \phi_x, \phi_y\}_j^T$) is composed of a displacement (u_z) and two angular displacements (ϕ_x, ϕ_y). The velocity vector ($\dot{\mathbf{u}}_j = d\mathbf{u}_j / dt = \{v_z, \omega_x, \omega_y\}_j^T$) consists of a linear velocity (v_z) and two angular velocities (ω_x, ω_y). The acceleration vector ($\ddot{\mathbf{u}}_j = d\dot{\mathbf{u}}_j / dt = \{a_z, \alpha_x, \alpha_y\}_j^T$) is composed of a linear acceleration (a_z) and two angular accelerations (α_x, α_y). The force vector of the node *j* ($\mathbf{f}_j = \{F_z, M_x, M_y\}_j^T$) consists of the forces (F_z) and the moments (M_x, M_y). Therefore, the displacement vector of the nodal line *i* ($\mathbf{U}_i = \{\mathbf{u}_1^T, \mathbf{u}_2^T, \cdots, \mathbf{u}_n^T\}_i^T$) is comprised of the displacement vectors of all nodes in the nodal line *i*. The force vector of the nodal line *i* ($\mathbf{F}_i = \{\mathbf{f}_1^T, \mathbf{f}_2^T, \cdots, \mathbf{f}_n^T\}_i^T$) consists of the force vectors of all nodes in the nodal line *i*.

If there are supporting parts that support some nodes of the plate from the base, they are modeled as 3 springs and 3 viscous dampers per node. The springs consist of a linear and two rotational springs of which the constants are $\hat{k}_z$, $\hat{K}_x$ and $\hat{K}_y$. The viscous dampers are comprised of a linear and two rotational viscous dampers of which the constants are $\hat{c}_z$, $\hat{C}_x$ and $\hat{C}_y$. In the present method, the boundary conditions of the left- and right-hand edges of the rectangular plate structure are modeled as springs and viscous dampers supporting the first and last nodal lines from the base. For example, the spring constants of nodal line 1 are considered as infinities in the case of a fixed condition at the left-hand edge. In the case of a free condition at the right-hand edge, the spring constants of nodal line *m*+1 are considered to be zeros.

If there are external forces acting on some nodes of the plate structure, they are modeled as an excitation force ($\hat{q}_z$) and two excitation moments ($\hat{Q}_x, \hat{Q}_y$) per node. When a node of the plate structure has an added mass, the added mass is considered to be an additional mass ($\hat{m}$) and two rotational inertias ($\hat{M}_x, \hat{M}_y$).

The strip i represents the i-th strip of the plate, which exists between the nodal line i and the nodal line i+1. Each strip has 2n nodes. We can easily obtain the mass matrix $\mathbf{M}_i$, the damping matrix $\mathbf{C}_i$ and the stiffness matrix $\mathbf{K}_i$ for the strip i by assembling the mass, damping and stiffness matrices of various plate elements such as the thin rectangular element with four node points, the thin triangular element with three node points, and so forth [14].

The equation of motion for the strip i at time t is represented as

$$\mathbf{M}_i\begin{Bmatrix}\ddot{\mathbf{U}}_i^L(t)\\ \ddot{\mathbf{U}}_i^R(t)\end{Bmatrix}+\mathbf{C}_i\begin{Bmatrix}\dot{\mathbf{U}}_i^L(t)\\ \dot{\mathbf{U}}_i^R(t)\end{Bmatrix}+\mathbf{K}_i\begin{Bmatrix}\mathbf{U}_i^L(t)\\ \mathbf{U}_i^R(t)\end{Bmatrix}=\begin{Bmatrix}\mathbf{F}_i^L(t)\\ \mathbf{F}_i^R(t)\end{Bmatrix}, \tag{1}$$

where $\dot{\mathbf{U}}_i(t)$ and $\ddot{\mathbf{U}}_i(t)$ are the velocity and acceleration vectors of the strip i at time t, respectively. Superscripts L and R represent the quantities of the left- and right-hand sides of a strip.

2.2 Newmark's method

From Newmark's method [13], the displacement and velocity vectors of the nodal line i at time t are assumed by using the acceleration vector at the same time and the displacement, velocity and acceleration vectors before time step Δt as follows:

$$\mathbf{U}_i(t)=\beta(\Delta t)^2\ddot{\mathbf{U}}_i(t)+\mathbf{Y}_i(t-\Delta t), \tag{2}$$

$$\dot{\mathbf{U}}_i(t)=\gamma\Delta t\ddot{\mathbf{U}}_i(t)+\mathbf{Z}_i(t-\Delta t), \tag{3}$$

where

$$\mathbf{Y}_i(t-\Delta t)=\mathbf{U}_i(t-\Delta t)+\Delta t\dot{\mathbf{U}}_i(t-\Delta t)+(0.5-\beta)(\Delta t)^2\ddot{\mathbf{U}}_i(t-\Delta t), \tag{4}$$

$$\mathbf{Z}_i(t-\Delta t)=\dot{\mathbf{U}}_i(t-\Delta t)+(1-\gamma)\Delta t\ddot{\mathbf{U}}_i(t-\Delta t), \tag{5}$$

and the parameters β and γ are chosen by considering the accuracy and stability of numerical integration.

2.3 Definition of mass coefficient matrix and force corrective vector

To easily describe the concept of the present method, a nodal line is divided analytically into the left- and right-hand sides of the nodal line. We denote quantities of the left-hand side of the nodal line with the head mark, –, on the symbols corresponding to the quantities. The quantities of the right-hand side of the nodal line are denoted without the head mark on the same symbols. Symbols with subscript i represent quantities corresponding to the nodal line i or the strip i.

We define the relationship between the force vector and the acceleration vector at the left- and right-hand sides of the nodal line i as follows:

$$\bar{\mathbf{F}}_i(\mathrm{t})=\bar{\mathbf{J}}_i\,\ddot{\bar{\mathbf{U}}}_i(\mathrm{t})+\bar{\mathbf{E}}_i(\mathrm{t}), \tag{6}$$

$$\mathbf{F}_i(\mathrm{t})=\mathbf{J}_i\,\ddot{\mathbf{U}}_i(\mathrm{t})+\mathbf{E}_i(\mathrm{t}), \tag{7}$$

where the matrices $\bar{\mathbf{J}}_i$ and $\mathbf{J}_i$ are termed the mass coefficient matrices at the left- and right-hand sides of the nodal line i, and the vectors $\bar{\mathbf{E}}_i(t)$ and $\mathbf{E}_i(t)$ are termed the force corrective vectors at the left- and right-hand sides of the nodal line i.

2.4 Transfer of mass coefficient matrix and force corrective vector

If there are added masses, springs, viscous dampers and external forces at the nodal line i, from the balancing of force vectors and the continuous condition of displacement vectors at the nodal line i, the following equations can be obtained.

$$\hat{\mathbf{M}}_i\ddot{\mathbf{U}}_i(t)=\hat{\mathbf{Q}}_i(t)+\mathbf{F}_i(t)-\bar{\mathbf{F}}_i(t)-\hat{\mathbf{C}}_i\dot{\mathbf{U}}_i(t)-\hat{\mathbf{K}}_i\mathbf{U}_i(t), \tag{8}$$

$$\mathbf{U}_i(t)=\bar{\mathbf{U}}_i(t),\quad \dot{\mathbf{U}}_i(t)=\dot{\bar{\mathbf{U}}}_i(t),\quad \ddot{\mathbf{U}}_i(t)=\ddot{\bar{\mathbf{U}}}_i(t), \tag{9}$$

where

$$\begin{aligned}\hat{\mathbf{M}}_i&=\mathrm{Diag}\,(\hat{m}_1,\hat{M}_{x1},\hat{M}_{y1},\hat{m}_2,\hat{M}_{x2},\hat{M}_{y2},\cdots,\hat{M}_{yn})_i,\\ \hat{\mathbf{C}}_i&=\mathrm{Diag}\,(\hat{c}_{z1},\hat{C}_{x1},\hat{C}_{y1},\hat{c}_{z2},\hat{C}_{x2},\hat{C}_{y2},\cdots,\hat{C}_{yn})_i,\\ \hat{\mathbf{K}}_i&=\mathrm{Diag}\,(\hat{k}_{z1},\hat{K}_{x1},\hat{K}_{y1},\hat{k}_{z2},\hat{K}_{x2},\hat{K}_{y2},\cdots,\hat{K}_{yn})_i,\\ \hat{\mathbf{Q}}_i&=\{\hat{q}_{z1},\hat{Q}_{x1},\hat{Q}_{y1},\hat{q}_{z2},\hat{Q}_{x2},\hat{Q}_{y2},\cdots,\hat{Q}_{yn}\}_i^T,\end{aligned} \tag{10}$$

in which Diag(⋯) refers to a diagonal matrix, and the matrices $\hat{\mathbf{M}}_i$, $\hat{\mathbf{K}}_i$ and $\hat{\mathbf{C}}_i$ denote the point mass, stiffness and damping matrices, respectively.

Consider the transfer of the mass coefficient matrix and the force corrective vector from the left-hand side of the nodal line i to the right-hand side of the nodal line i. We can derive the matrix $\mathbf{J}_i$ and the vector $\mathbf{E}_i(t)$ from Eqs. (2) and (3), and from Eqs. (6) - (9) as follows:

$$\mathbf{J}_i = \bar{\mathbf{J}}_i + \hat{\mathbf{M}}_i + \gamma\Delta t\hat{\mathbf{C}}_i + \beta(\Delta t)^2\hat{\mathbf{K}}_i, \tag{11}$$

$$\mathbf{E}_i(t) = \bar{\mathbf{E}}_i(t) - \hat{\mathbf{Q}}_i(t) + \hat{\mathbf{C}}_i\,\mathbf{Z}_i(t-\Delta t) + \hat{\mathbf{K}}_i\mathbf{Y}_i(t-\Delta t), \tag{12}$$

where Eqs. (11) and (12) are the point transfer rules of the mass coefficient matrix and the force corrective vector, respectively.

Because the left-hand side of the strip *i* becomes the right-hand side of the nodal line *i*, and the right-hand side of the strip *i* becomes the left-hand side of the nodal line *i*+1, the following equations are obtained by substituting Eqs. (2) and (3) for Eq. (1).

$$\mathbf{A}_i\ddot{\mathbf{U}}_i(t) + \mathbf{B}_i\bar{\ddot{\mathbf{U}}}_{i+1}(t) + \mathbf{W}_i(t) = -\mathbf{F}_i(t), \tag{13}$$

$$\mathbf{C}_i\ddot{\mathbf{U}}_i(t) + \mathbf{D}_i\bar{\ddot{\mathbf{U}}}_{i+1}(t) + \bar{\mathbf{W}}_{i+1}(t) = \bar{\mathbf{F}}_{i+1}(t), \tag{14}$$

where

$$\begin{bmatrix}\mathbf{A}_i & \mathbf{B}_i\\ \mathbf{C}_i & \mathbf{D}_i\end{bmatrix} = \mathbf{M}_i + \gamma\Delta t\mathbf{C}_i + \beta(\Delta t)^2\mathbf{K}_i,$$
$$\begin{Bmatrix}\mathbf{W}_i(t)\\ \bar{\mathbf{W}}_{i+1}(t)\end{Bmatrix} = \mathbf{C}_i\begin{Bmatrix}\mathbf{Z}_i(t-\Delta t)\\ \bar{\mathbf{Z}}_{i+1}(t-\Delta t)\end{Bmatrix} + \mathbf{K}_i\begin{Bmatrix}\mathbf{Y}_i(t-\Delta t)\\ \bar{\mathbf{Y}}_{i+1}(t-\Delta t)\end{Bmatrix},$$
$$\begin{Bmatrix}\mathbf{U}_i(t)\\ \bar{\mathbf{U}}_{i+1}(t)\end{Bmatrix} = \begin{Bmatrix}\mathbf{U}_i^L(t)\\ \mathbf{U}_i^R(t)\end{Bmatrix}, \quad \begin{Bmatrix}\mathbf{F}_i(t)\\ \bar{\mathbf{F}}_{i+1}(t)\end{Bmatrix} = \begin{Bmatrix}-\mathbf{F}_i^L(t)\\ \mathbf{F}_i^R(t)\end{Bmatrix}. \tag{15}$$

Consider the transfer of the mass coefficient matrix and the force corrective vector from the right-hand side of the nodal line *i* to the left-hand side of the nodal line *i*+1, across the strip *i*. We can derive the matrix $\bar{\mathbf{J}}_{i+1}$ and the vector $\bar{\mathbf{E}}_{i+1}(t)$ from the equation substituted with *i*=*i*+1 in Eq. (6), and from Eqs. (7), (13) and (14) as follows:

$$\bar{\mathbf{J}}_{i+1} = \mathbf{C}_i\,\mathbf{V}_i + \mathbf{D}_i, \tag{16}$$

$$\bar{\mathbf{E}}_{i+1}(t) = \mathbf{C}_i\,\mathbf{H}_i(t) + \bar{\mathbf{W}}_{i+1}(t), \tag{17}$$

where

$$\mathbf{V}_i = \mathbf{G}_i\mathbf{B}_i, \quad \mathbf{G}_i = -(\mathbf{J}_i + \mathbf{A}_i)^{-1},$$
$$\mathbf{H}_i(t) = \mathbf{G}_i\{\mathbf{W}_i(t) + \mathbf{E}_i(t)\}, \tag{18}$$

and Eqs. (16) and (17) are the field transfer rules of the mass coefficient matrix and the force corrective vector, respectively.

2.5 Transient response

Because the boundary condition at the left-hand edge is modeled as the point mass, stiffness and damping matrices at nodal line 1 in the present method, the force vector $\bar{\mathbf{F}}_1(t)$ at the left-hand side of nodal line 1 can be considered a null vector. We can determine the matrix $\mathbf{J}_1$ and the vector $\mathbf{E}_1(t)$ from $\bar{\mathbf{F}}_1(t) = \mathbf{0}$ and Eqs. (2), (3), (7) and (8) into which *i*=1 has been substituted as follows:

$$\mathbf{J}_1 = \hat{\mathbf{M}}_1 + \gamma\Delta t\hat{\mathbf{C}}_1 + \beta(\Delta t)^2\hat{\mathbf{K}}_1, \tag{19}$$

$$\mathbf{E}_1(t) = \hat{\mathbf{C}}_1\mathbf{Z}_1(t-\Delta t) + \hat{\mathbf{K}}_1\mathbf{Y}_1(t-\Delta t) - \hat{\mathbf{Q}}_1(t). \tag{20}$$

We can finally derive the matrix $\mathbf{J}_{m+1}$ and the vector $\mathbf{E}_{m+1}(t)$ when successively applying the above transfer rules, using Eqs. (11), (12), (16) and (17), after first obtaining the matrix $\mathbf{J}_1$ and the vector $\mathbf{E}_1(t)$ from Eqs. (19) and (20).

Since the boundary condition at the right-hand edge of the plate structure is modeled as the point mass, stiffness and damping matrices at nodal line *m*+1, the right-hand side of nodal line *m*+1 can be considered analytically as being free, that is, $\mathbf{F}_{m+1}(t) = \mathbf{0}$. From $\mathbf{F}_{m+1}(t) = \mathbf{0}$ and Eq. (7), into which *i*=*m*+1 has been substituted, the acceleration vector of nodal line *m*+1 can be obtained as follows:

$$\ddot{\mathbf{U}}_{m+1}(t) = -\mathbf{J}_{m+1}^{-1}\,\mathbf{E}_{m+1}(t). \tag{21}$$

From Eq. (7), (9), (13) and (18), the relationship of the acceleration vectors, across the strip *i,* is given as

$$\ddot{\mathbf{U}}_i(t) = \mathbf{V}_i\ddot{\mathbf{U}}_{i+1}(t) + \mathbf{H}_i(t). \tag{22}$$

After the acceleration vector of nodal line *m*+1 is calculated from Eq. (21), the acceleration vectors at the other nodal lines can be obtained recursively by using Eq. (22).

2.6 Initial acceleration

The point transfer rules of the mass coefficient matrix and the force corrective vector at the initial time can be obtained from Eqs. (6) - (9) at *t*=0 as follows:

$$\mathbf{J}_i = \bar{\mathbf{J}}_i + \hat{\mathbf{M}}_i, \tag{23}$$

$$\mathbf{E}_i(0) = \bar{\mathbf{E}}_i(0) - \hat{\mathbf{Q}}_i(0) + \hat{\mathbf{C}}_i\,\dot{\mathbf{U}}_i(0) + \hat{\mathbf{K}}_i\mathbf{U}_i(0). \tag{24}$$

From Eqs. (1) and (15) at t=0, the following equation can be obtained.

$$\tilde{\mathbf{A}}_i\ddot{\mathbf{U}}_i(0)+\tilde{\mathbf{B}}_i\ddot{\bar{\mathbf{U}}}_{i+1}(0)+\mathbf{W}_i(0)=-\mathbf{F}_i(0), \tag{25}$$

$$\tilde{\mathbf{C}}_i\ddot{\mathbf{U}}_i(0)+\tilde{\mathbf{D}}_i\ddot{\bar{\mathbf{U}}}_{i+1}(0)+\bar{\mathbf{W}}_{i+1}(0)=\bar{\mathbf{F}}_{i+1}(0), \tag{26}$$

where

$$\begin{bmatrix}\tilde{\mathbf{A}}_i & \tilde{\mathbf{B}}_i\\ \tilde{\mathbf{C}}_i & \tilde{\mathbf{D}}_i\end{bmatrix}=\mathbf{M}_i,\qquad \begin{Bmatrix}\mathbf{W}_i(0)\\ \bar{\mathbf{W}}_{i+1}(0)\end{Bmatrix}=\mathbf{C}_i\begin{Bmatrix}\dot{\mathbf{U}}_i(0)\\ \dot{\bar{\mathbf{U}}}_{i+1}(0)\end{Bmatrix}+\mathbf{K}_i\begin{Bmatrix}\mathbf{U}_i(0)\\ \bar{\mathbf{U}}_{i+1}(0)\end{Bmatrix}. \tag{27}$$

The field transfer rules of the mass coefficient matrix and the force corrective vector at the initial time can be obtained from the equation substituted with i=i+1 in Eq. (6) at t=0, and from Eqs. (7), (25) and (26) at t=0 as follows:

$$\bar{\mathbf{J}}_{i+1}=\tilde{\mathbf{C}}_i\tilde{\mathbf{V}}_i+\tilde{\mathbf{D}}_i, \tag{28}$$

$$\bar{\mathbf{E}}_{i+1}(0)=\tilde{\mathbf{C}}_i\tilde{\mathbf{H}}_i(0)+\bar{\mathbf{W}}_{i+1}(0), \tag{29}$$

where

$$\tilde{\mathbf{V}}_i=\tilde{\mathbf{G}}_i\tilde{\mathbf{B}}_i,\quad \tilde{\mathbf{G}}_i=-(\mathbf{J}_i+\tilde{\mathbf{A}}_i)^{-1},\qquad \tilde{\mathbf{H}}_i(0)=\tilde{\mathbf{G}}_i\{\mathbf{W}_i(0)+\mathbf{E}_i(0)\}. \tag{30}$$

From Eqs. (7) and (8) into which i=1 has been substituted at t=0, we can determine the matrix $\mathbf{J}_1$ and the vector $\mathbf{E}_1(0)$ as follows:

$$\mathbf{J}_1=\hat{\mathbf{M}}_1, \tag{31}$$

$$\mathbf{E}_1(0)=\hat{\mathbf{C}}_1\dot{\mathbf{U}}_1(0)+\hat{\mathbf{K}}_1\mathbf{U}_1(0)-\hat{\mathbf{Q}}_1(0). \tag{32}$$

After determining the matrix $\mathbf{J}_1$ from Eq. (31), we can successively apply Eqs. (23) and (28) for plate structures. We can then obtain the matrix $\mathbf{J}_{m+1}$. In the same manner, after obtaining the vector $\mathbf{E}_1(0)$ from Eq. (32), we can successively apply Eqs. (24) and (29). We can then obtain vector $\mathbf{E}_{m+1}(0)$.

From Eqs. (7), (9), (18) and (25) at t=0, the relationship of the acceleration vectors between the left- and right-hand sides of the strip i is given as

$$\ddot{\mathbf{U}}_i(0)=\tilde{\mathbf{V}}_i\ddot{\mathbf{U}}_{i+1}(0)+\tilde{\mathbf{H}}_i(0). \tag{33}$$

The initial acceleration vector of nodal line m+1 can be obtained from Eq. (21) at t=0. The initial acceleration vectors at the other nodal lines can be obtained recursively by using Eq. (33).

3. Verification and discussion

To verify the computational accuracy and efficiency of the finite element-transfer mass coefficient method (FE-TMCM), the authors made three computer programs based on the finite element method (FEM), the finite element-transfer matrix method (FE-TMM) and the FE-TMCM for calculating the transient responses of rectangular plate structures on a personal computer. In the numerical calculation, the FEM refers to the direct integration method [15], and the FE-TMM denotes the standard FE-TMM that does not have special techniques to partly avoid round-off errors [3].

Several rectangular plate structures were chosen as numerical models. The thin rectangular element with four node points [14] was used in the computer programs. The dynamic responses and computation times obtained by the FE-TMCM were compared with those obtained by the FEM and the FE-TMM under the same conditions.

3.1 Example 1

The first numerical model is a cantilever square plate structure with a viscous damper at the apex of the square plate, as shown in Fig. 3. The damping coefficient of the viscous damper ($\hat{c}_z$) is 50 Ns/m.

The plate structure is subjected to a triangular impulsive load expressed by: $\hat{q}_z(t)$=10 (1-t/0.05) N, t < 0.05 sec, as shown in Fig. 3. The physical and geometrical properties of the plate are as follows: 1 m length, 1 m width, 0.005 m thickness, 7850 kg/m^3 mass density, 206 GPa elastic modulus and 0.3 Poisson's ratio. The structural damping of the plate is neglected. Parameters β and γ of Newmark's method are 0.25 and 0.5, respectively.

When the time step Δt is 0.0005 s and the plate is divided into 2×2, 4×4, 6×6, 8×8 and 10×10 mesh patterns, the transient responses of the plate structure were computed by the above three methods. In the case of the 2×2 and 4×4 mesh patterns, the transient responses of the plate structure obtained by the FE-TMM agreed well with those obtained by the FEM. In the case of the 6×6, 8×8 and 10×10 mesh patterns, the FE-TMM produced numerically unstable results

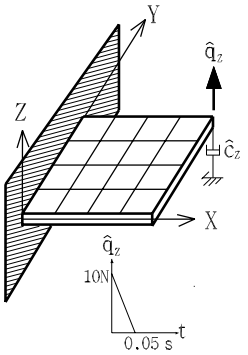

Fig. 3. Cantilever square plate structure.

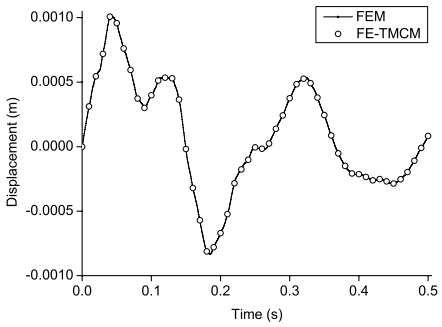

Fig. 4. Transient response of cantilever square plate structure (10×10 mesh pattern, Δt = 0.0005 s).

that were meaningless. However, under each mesh pattern, the transient responses obtained by the FE-TMCM fully agreed with those obtained by the FEM. Fig. 4 shows the dynamic responses of the excitation point of the structure obtained by the FEM and the FE-TMCM, when the plate is divided into the 10×10 mesh pattern. To distinctly compare the response results of both methods in Fig. 4, the result of the FEM is represented by the solid line, and that of the FE-TMCM is expressed as only 51 symbols, because the number of time points of the response is very large and both results coincide with each other. The results of the FE-TMCM in Fig. 5, Fig. 7 and Fig. 8 are expressed as only 51 symbols, for the same reason as Fig. 4.

Table 1 shows computation times by the three methods according to the mesh pattern. It can be seen from Table 1 that while the FE-TMCM is not particularly useful for plate structures that are modeled as a very small number of plate elements, it is significantly useful for plate structures that are modeled as a large number of plate elements in terms of computation time.

Table 1. Comparison of computation times for cantilever square plate structure (unit: s).

Mesh	FEM	FE-TMCM	FE-TMM
2×2	0.427	0.578	0.953
4×4	2.172	1.469	2.646
6×6	8.151	3.052	-----
8×8	28.057	5.719	-----
10×10	77.927	9.839	-----

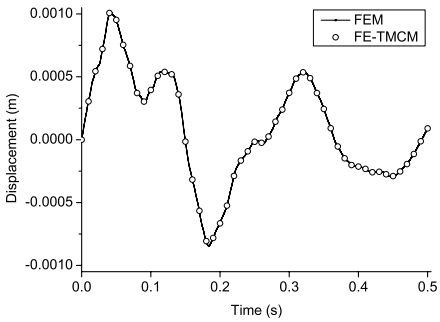

Fig. 5. Transient response of cantilever square plate structure (4×4 mesh pattern, Δt = 0.0001 s).

When the plate is divided into the 4×4 mesh pattern and the time steps are 0.0010 s, 0.0005 s, 0.0003 s and 0.0001 s, the transient responses of the structure were computed by the three methods. In the case of the time steps of 0.0010 s and 0.0005 s, the transient responses of the plate structure obtained by the FE-TMM agreed well with those obtained by the FEM. In the case of the time steps of 0.0003 s and 0.0001 s, the FE-TMM produced unstable and meaningless results. However, under every time step, the transient responses of the plate structure obtained by the FE-TMCM coincided completely with those obtained by the FEM. Therefore, we confirmed that the FE-TMCM is superior to the FE-TMM in terms of computational accuracy. Fig. 5 shows the transient response at the excitation point of the plate structure for the FEM and the FE-TMCM, when the time step is 0.0001 s. In Fig. 5, we confirmed that the results of both methods also coincide.

When the plate is modeled as the 10×10 mesh pattern, the total degrees-of-freedom of the plate is 363. In the FEM, the sizes of the system mass, damping and stiffness matrices are then 363 by 363. However, the size of the mass coefficient matrix in the FE-TMCM is only 33 by 33. Therefore, the FE-TMCM is superior to the FEM in terms of the management of computation memory, because the FE-TMCM uses

the small matrix size through the transfer rules

3.2 Example 2

The second numerical model is a rectangular plate structure supported with springs and viscous dampers, as shown in Fig. 6. The spring constants of the springs ($\hat{k}_{z,c}$) and the damping coefficient of the viscous dampers ($\hat{c}_{z,c}$) at the four apexes of the rectangular plate are 1.0e4 N/m and 100 Ns/m, respectively. The plate structure is subjected to a step load, $\hat{q}_z(t)$=10 N, at the center. The physical and geometrical properties of the plate are as follows: 1 m length, 0.5 m width, 0.005 m thickness, 2700 kg/m^3 mass density, 70 GPa elastic modulus and 0.33 Poisson's ratio. The structural damping of the plate is neglected. Parameters β and γ of Newmark's method are 0.25 and 0.5, respectively.

When the time step is 0.0005 s, the spring constants of the intermediate springs ($\hat{k}_{z,m}$) are 1.0e4 N/m, and the plate is divided into 4×2, 8×4, 12×6, 16×8 and 20×10 mesh patterns, the transient responses of the structure were computed by the above three methods. In the case of the 4×2 mesh pattern, the transient responses of the structure obtained by the FE-TMM agreed well with those obtained by the FEM. In the case of the 8×4, 12×6, 16×8 and 20×10 mesh patterns, the FE-TMM produced numerically unstable and meaningless results.

However, under every mesh pattern, the transient responses of the plate structure obtained by the FE-TMCM fully agreed with those obtained by the FEM. Fig. 7 shows the transient responses at the center of the plate structure obtained by the FEM and the FE-TMCM when the plate is divided into the 20×10 mesh pattern. In Fig. 7, we confirmed that the results of the FEM and the FE-TMCM also coincide.

Table 2 shows the computation time according to the mesh pattern for the three methods. It can be seen that the FE-TMCM is superior to the FEM in terms of computation time in the case of computing transient responses of plate structures modeled as a large number of plate elements.

When the plate is divided into the 4×2 mesh pattern, the time step is 0.0005 s and the spring constants of the intermediate springs ($\hat{k}_{z,m}$) are 1.0e4 N/m, 1.0e7 N/m and 1.0e10 N/m, the transient responses of the structure were computed by the three methods. In the case of the spring constants of 1.0e4 N/m and 1.0e7 N/m, the transient responses of the plate structure obtained by the FE-TMM agreed well with those obtained by the FEM. In the case of the spring constant of 1.0e10 N/m, the FE-TMM produced unstable and meaningless results. However, under each spring constant, the transient responses obtained by the FE-TMCM fully agreed with those obtained by the FEM. Fig. 8 shows the transient response at the center of the plate structure obtained by the FEM and the FE-TMCM when the spring constants of the intermediate springs are 1.0e10 N/m. In Fig. 8, we confirmed that the results of both methods also coincide.

When the plate is modeled as the 20×10 mesh pattern, the total degrees-of-freedom of the numerical model is 693. In the FEM, the sizes of the system mass, damping and stiffness matrices are then 693 by

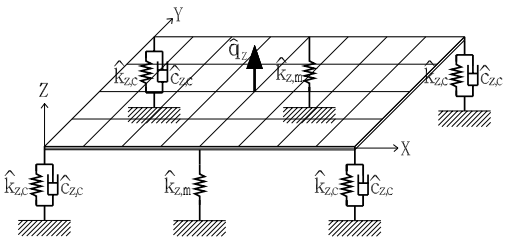

Fig. 6. Rectangular plate structure supported by springs and viscous dampers.

Table 2. Comparison of computation times for rectangular plate supported by springs and viscous dampers (unit: s).

Mesh	FEM	FE-TMCM	FE-TMM
4×2	0.859	0.969	1.625
8×4	6.969	2.719	-----
12×6	37.440	5.844	-----
16×8	118.917	11.239	-----
20×10	292.661	19.750	-----

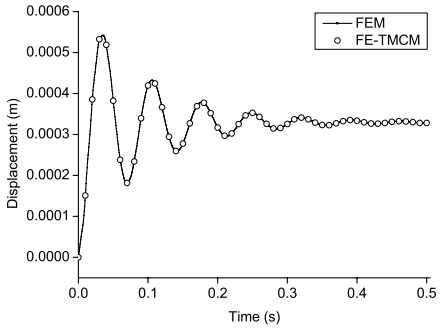

Fig. 7. Transient response of rectangular plate structure supported by springs and viscous dampers (20×10 mesh pattern, Δt = 0.0005 s, $k_{z,m}$ = 1.0e4 N/m).

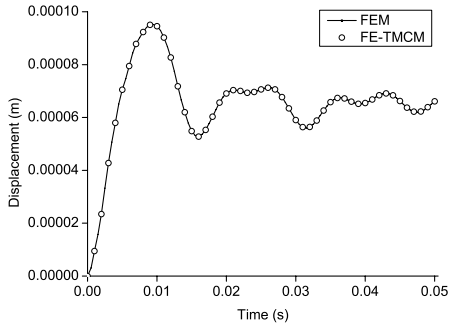

Fig. 8. Transient response of rectangular plate structure supported by springs and viscous dampers (4×4 mesh pattern, Δt = 0.0005 s, $\hat{k}_{z,m}$ = 1.0e10 N/m).

693. However, the size of the mass coefficient matrix in the FE-TMCM is only 33 by 33. Therefore, the FE-TMCM is superior to the FEM in terms of the management of computation memory, particularly, for the case where the length of the plate is longer than the width.

The FEM requires a large computation memory and a long computation time when the transient response of the rectangular plate structure with very large degrees-of-freedom is analyzed. However, the FE-TMCM can significantly reduce the computation time without the loss of accuracy, in spite of using a small computation memory, by using the transfer rules successively

4. Conclusions

A new transient response analysis algorithm, the finite element-transfer mass coefficient method, was developed in order to significantly reduce the computational time and memory in the transient analysis of a rectangular plate structure comprised of a large number of plate elements. The concept of the finite element-transfer mass coefficient method was based on the combination of the transfer technique of the transfer mass coefficient method, the modeling technique of the finite element method, and the numerical integration technique of Newmark's method.

Through the results of the transient analysis for several numerical models, we can verify that the FEM requires long computation time and large computation memory when a rectangular plate structure that consists of a large number of plate elements is analyzed. Furthermore, the FE-TMM has many drawbacks in the transient analysis when the time step of numerical integration is short and the plate structure is comprised of many plate elements or supported by rigid springs at the intermediate of the plate structure. However, the FE-TMCM can considerably reduce the computation time without the loss of accuracy, in spite of using small computation memory, by using the transfer rules successively.

In this paper, the developed computational algorithm is limited to two-dimensional structures such as lattice and plate structures. Therefore, the authors will study in the future to develop an efficient computation algorithm for the transient analysis of complex three-dimensional structures.

References

[1] M. A. Dokainish, New approach for plate vibration: combination of transfer matrix and finite-element technique, *Trans. ASME Journal of Engineering for Industry*, 94 (1972) 526-530.

[2] A. S. Kumar and T. S. Sankar, A new transfer matrix method for response analysis of large dynamic systems, *Computers & Structures*, 23 (4) (1986) 545-552.

[3] M. Ohga and T. Shigematsu, Transient analysis of plates by a combined finite element-transfer matrix method, *Computers & Structures*, 26 (4) (1987) 543-549.

[4] N. S. Sehmi, *Large order structural eigenanalysis techniques algorithm for finite element systems*, John Wiley & Sons, New York, USA, (1989).

[5] M. Ohga, T. Shigematsu, and T. Hara, A finite element-transfer matrix method for dynamic analysis of frame structures, *Journal of Sound and Vibration*, 167 (3) (1993) 401-411.

[6] H. Xue, A combined finite element-Riccati transfer matrix method in frequency domain for transient structural response, *Computers & Structures*, 62 (2) (1997) 215-220.

[7] D. H. Moon and M. S. Choi, Vibration analysis for frame structures using transfer of dynamic stiffness coefficient, *Journal of Sound and Vibration*, 234 (5) (2000) 725-736.

[8] A. S. Ashour and A. M. Farag, A combination between Laplace transform, strip method and transition matrix for determination of dynamic response and damping effect of plates, *International Journal of Acoustics and Vibration*, 5 (4) (2000) 191-195.

[9] M. S. Choi, Free vibration analysis of plate structures using finite element-transfer stiffness coeffi-

cient method, *KSME International Journal*, 17 (6) (2003) 805-815.
[10] Y. Bonkobara, T. Kondou, T. Ayabe and M. S. Choi, Vibration analysis of a frame structure by generalized transfer stiffness coefficient mehod, *Journal of System Design and Dynamics*, 1 (1) (2007) 73-84.
[11] M. S. Choi, D. J. Yeo, J. H. Byun, J. J. Suh and J. K. Yang, Development of dynamic analysis algorithm for beam structures using transfer of mass coefficient, *Journal of Mechanical Science and Technology*, 23 (2009) 389-400.
[12] E. C. Pestel and F. A. Leckie, *Matrix methods in elastomechanics*, McGraw-Hill, New York, USA, (1963).
[13] L. L. Logan, *A first course in the finite element method using Algor*, PWS, Boston, USA, (1993) 740-752.
[14] M. Petyt, *Introduction to finite element vibration analysis*, Cambridge University Press, Cambridge, England, (1990) 229-244.
[15] K. J. Bathe, *Finite element procedures*, Prentice-Hall, New Jersey, USA, (1996).

Myung-Soo Choi received his B.S. and M.S. degrees from National Fisheries University of Pusan, Korea, in 1992 and 1994, respectively. He then received his Ph.D. degree from Pukyong National University in 1999. Dr. Choi is currently an Assistant Professor at the Department of Maritime Police Science at Chonnam National University in Yeosu, Korea. His research interests include mechanical vibration, structural dynamics, and optimum design.

Duck-Jong Jang received his B.S. and M.S. degrees from National Fisheries University of Yosu, in 1993 and 1995, respectively. He then received his Ph.D. degree from Pukyong National University in 2002. Dr. Jang is currently an Assistant Professor at the Department of Maritime Police Science at Chonnam National University in Yeosu, Korea. His research interests include marine safety, numerical analysis, fluid kinematic, and spilled oil response system design.

Young-Bok Kim received his B.S. and M.S. in Maritime Engineering from National Fisheries University of Pusan, Korea, in 1989 and 1991, respectively. He then received his Ph.D. degree from Kobe University, Japan in 1996. Dr. Kim is currently a Professor at the School of Mechanical Engineering at Pukyong National University in Busan, Korea. His research interests include control theory and application with dynamic ship positioning and crane control system design etc.

Ji-Seong Jang received his B.S. and M.S. degrees from National Fisheries University of Pusan, Korea, in 1990 and 1994, respectively. He then received his Ph.D. degree from Tokyo Institute of Technology in 1998. Dr. Jang is currently an Associate Professor at the School of Mechanical Engineering at Pukyong National University in Busan, Korea. His research interests include pneumatic driving system, flow measurement of compressible fluid, and optimum design.

Deok-Hong Moon received his B.S. degree from National Fisheries University of Pusan, in 1973 and M.S. in Engineering from Korea Maritime University, in 1981. He then received Ph.D. degree from Kyushu University in 1990. Dr. Moon is currently a Professor at the School of Mechanical Engineering at Pukyong National University in Busan, Korea. His research interests include mechanical vibration, structural analysis techniques, vibroacoustic stimulation, and human vibration.